Chinese Chemical Letters 35 (2024) 109231

Contents lists available at ScienceDirect

Chinese Chemical Letters

journal homepage: www.elsevier.com/locate/cclet

Highly stable side-chain-type cardo poly(aryl ether ketone)s membranes for vanadium flow battery

Ziming Zhao[a,b,c], Qing Dai[c], Sihan Huang[a,b], Wenjing Lu[c], Yaohan Chen[a], Jifu Zheng[a], Suobo Zhang[a], Shenghai Li[a,b,*], Xianfeng Li[c,*]

[a] Key Laboratory of Polymer Ecomaterials, Changchun Institute of Applied Chemistry, Chinese Academy of Sciences, Changchun 130022, China
[b] School of Applied Chemistry and Engineering, University of Science and Technology of China, Hefei 230026, China
[c] Division of Energy Storage, Dalian National Laboratory for Clean Energy, Dalian Institute of Chemical Physics, Chinese Academy of Sciences, Dalian 116023, China

ARTICLE INFO

Article history:
Received 12 August 2023
Revised 17 October 2023
Accepted 20 October 2023
Available online 24 October 2023

Keywords:
Vanadium flow battery
Energy storage technology
Ion exchange membrane
Ion transport mechanism
Poly(arylene ether ketone)s (PAEKs)

ABSTRACT

Vanadium flow batteries (VFBs) have drawn considerable attention as an emerging technology for large-scale energy storage systems (ESSs). One of the pivotal challenges is the availability of eligible ion exchange membranes (ICMs) that provide high ion selectivity, proton conductivity, and stability under rigorous condition. Herein, a 'side-chain-type' strategy has been employed to fabricate highly stable phenolphthalein-based cardo poly(arylene ether ketone)s (PAEKs) membrane with low area resistance (0.058 Ω cm^2), in which flexible alkyl spacers effectively alleviated inductive withdrawing effect from terminal ion exchange groups thus enabling a stable backbone. The assembled VFBs based on PAEKs bearing pendent alkyl chain terminated with quaternary ammonium (Q-PPhEK) demonstrated an energy efficiency above 80% over 700 cycles at 160 mA/cm^2. Such a remarkable results revealed that the side-chain-type strategy contributed to enhancing the ICMs stability in strong oxidizing environment, meanwhile, more interesting backbones would be woken with this design engaging in stable ICMs for VFBs.

Increasing energy demands and environmental concerns are current cynosure, which have been surged into energy development propelling global energy reframing towards renewable energy system, such as wind power and solar energy [1–3]. As renewable energy resource has been tagged with intermittence which mismatches between electricity generated and corresponding demand, large-scale energy storage systems (ESSs) can effectively mitigate the limitation [4–6]. Vanadium flow batteries (VFBs), one of typical ESSs, are feasible and prevail all over the world with successful commercialization by virtue of independent regulation of power and capacity together with high safety and long lifetime [4,7–9]. As one of the most mature flow battery technologies, VFBs further development of the battery is limited by the stability and cost of the membrane.

Ion-conducting membranes (ICMs), the key component of VFBs, separates catholytes and anolytes while conducts charge carriers to make the circuit complete [7,10–13]. ICMs including dense membranes and porous membranes, in which dense membranes includes cation exchange membranes (CEMs) with negatively charged groups, anion exchange membrane (AEMs) with positively charged groups and amphoteric ion exchange membranes (AIEMs) with both negatively and positively charged groups [10,14]. The battery performance, such as coulombic efficiency (CE), voltage efficiency (VE) and energy efficiency (EE) are highly affected by the selectivity and conductivity of ICMs [7,10,15–18]. Hence, the design of the high stability, selectivity, conductivity, and low-cost membrane has become one of the most important issues for VFBs development.

One intractable thing should be noted that the VFBs electrolyte comprising strong oxidant and acid, which poses instability and decomposition concerns for ICMs [19–21]. VO_2^+ species are strongly oxidative especially in acid environment, which would cause serious chemical decomposition of polymers. To meet the requirements for VFBs application especially used in rigorous environment, membranes always be asked for elite stability. The most commonly used VFBs membrane is perfluorosulfonic acid cation exchange membrane (such as Nafion series), whose stable and hydrophobic C-F bonds tightly surround the polymer backbone to prevent attack and degradation while hydrophilic sulfonic groups gather into ion clusters for ion conduction [15,22–28]. However, Nafion has encountered the bottlenecks of low selectivity and high

* Corresponding authors.
E-mail addresses: lsh@ciac.ac.cn (S. Li), lixianfeng@dicp.ac.cn (X. Li).

https://doi.org/10.1016/j.cclet.2023.109231
1001-8417/

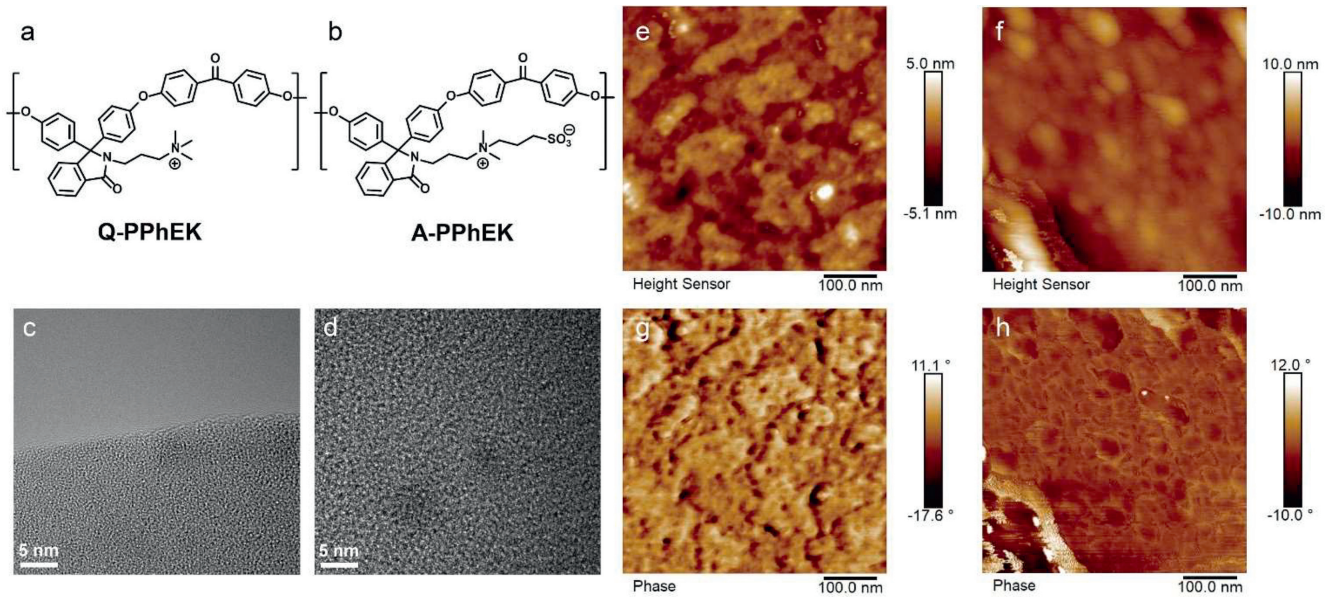

Fig. 1. Chemical structure, TEM images, AFM height images, and Phase images of (a, c, e, and g) Q-PPhEK and (b, d, f, and h) A-PPhEK membranes.

cost, which slows the pace of VFBs development. There is an urgent demand designing high-performance membranes with acceptable selectivity, conductivity, stability and cost for VFBs. Since most nonfluorinated polymer always cannot endure such rigorous condition, membrane design should be focus on inert materials with considerable stability [20].

Cardo poly(arylene ether ketone) (PAEK) is widely used as polymer membranes due to its impressive physical and chemical stability [29–32]. Normally, the semicrystalline PAEK has considerable hydrophobicity and it is not solution processible [33,34]. Hence hydrophilic modification should be executed to alleviate the membrane resistance and make PAEK capable for VFBs.

Herein, we propose two functionalized phenolphthalein-based cardo poly(arylene ether ketone)s bearing pendent alkyl chain terminated with quaternary ammonium, Q-PPhEK (Fig. 1a), and zwitterionic group, A-PPhEK (Fig. 1b), respectively *via* a typical polycondensation for VFBs as shown in Fig. S1 (Supporting information) [35,36]. These side-chain-type ion exchange membranes exhibit impressive robustness under rigorous condition as the ion exchange groups are separated by the alkyl spacers. Electron withdrawing effect from quaternary ammonium and sulfonic acid groups can be effectively retarded by alkyl spacers which contribute to the stable backbone especially for the sensitive moiety (ether and carbonyl group) [37–39]. Based on this design, both phenolphthalein-based ICMs demonstrate comparable stability with Nafion at lower cost. Furthermore, Q-PPhEK membrane delivers a satisfying area resistance and the assembled VFB batteries also show outstanding long-term cycling performance (over 700 cycles with EE of 80% at 160 mA/cm^2). More polymer by the 'side-chain-type' strategy will be taken into consideration for VFBs.

The phenolphthalein-based cardo polymers were prepared by a typical nucleophilic substitution polycondensation of lactamized phenolphthalein and 4,4′-difluorobenzophenone catalyzed by potassium carbonate (Fig. S1). The chemical structure of anion exchange membrane (Q-PPhEK) and amphoteric membrane (A-PPhEK) were verified by ^{1}H NMR spectroscopy (Figs. S2 and S3 in Supporting information) and the corresponding basic properties of all the phenolphthalein-based membranes including thickness, ion exchange capacity (IEC), tensile strength, WU, SR and area resistance (R_A) are shown in Table S1 (Supporting information). The characteristic peaks of the aromatic proton from 7.0 ppm to 9.0 ppm and the alkyl protons of side chains at *ca.* 0.8 ppm to 3.6 ppm in ^{1}H NMR spectra confirmed that the pendant ion exchange group had been successfully incorporated (Figs. S2 and S3). The tensile strength of Q-PPhEK (44.9 MPa) is comparable with commercial Nafion 115 which indicates it is candidate for VFBs operating under the condition requiring high mechanical properties. While the tensile strength of A-PPhEK is only 26.4 MPa as its relatively large proportion of long side chains and ion exchange groups. WU of Q-PPhEK (36.2%) in DI water is higher than A-PPhEK (17.4%) which may ascribe to different membrane microstructure and ionic cross-linked network of cation-exchange groups (sulfonic acid) and anion-exchange groups (quaternary ammonium) [40–43]. Apparently, the same trend was observed in SR. A much lower R_A of Q-PPhEK (0.058 Ω cm^2) and a relatively low one of A-PPhEK (0.176 Ω cm^2) are obtained by four-probe method in a H-cell which may cause by the different SR. The hydrophilicity of Q-PPhEK and A-PPhEK have been measured as 66.8° and 67.4° respectively by water contact angle (WCA) (Fig. S4 in Supporting information). In addition to the Q-PPhEK and A-PPhEK, the sulfonic group and double quaternary ammonium groups modified phenolphthalein cardo PAEKs were also synthesized, respectively (Figs. S5 and S6 in Supporting information). However, the poor hydrophilicity (WCA = 85.4°) of the sulfonic group decorated PAEK led to a higher R_A and maynot be used in VFBs (Fig. S7 in Supporting information). While the double quaternary ammonium group decorated PAEK suffered from a severe swelling even dissolved in the water.

The surface morphology and the distribution of ion exchange groups are shown in typical TEM images (Figs. 1c and d). The dark region is attributed to the hydrophilic domains dyed by $PdCl_4^-$ or Pb^{2+} stems from opposite charge attraction while the light region represents hydrophobic polymer backbones. The TEM image displays that the aliphatic side chains terminated with ion exchange groups could aggregate into hydrophilic clusters, *i.e.,* ion channels. In addition, a clear N/S mapping of quaternary ammonium/sulfonated groups enable by high resolution transmission electron microscope (HRTEM), which indicates that the functional groups have been successfully incorporated into phenolphthalein-based polymer (Figs. S8 and S9 in Supporting information).

In addition, the surface morphology of PPhEK membranes has been further verified by atomic force microscope (AFM) images.

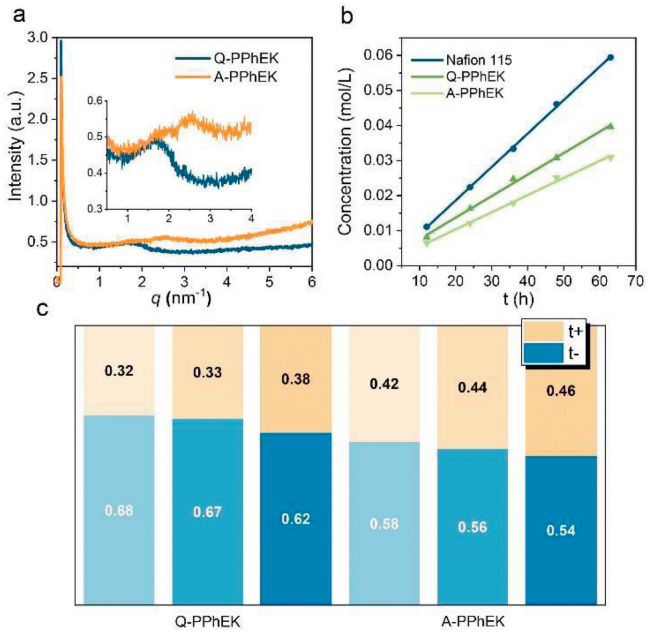

Fig. 2. Structure-activity relationship of ion cluster and ion transport. (a) SAXS curves of Q-PPhEK and A-PPhEK. (b) VO^{2+} permeation test of Q-PPhEK and A-PPhEK. (c) ITN of KCl in Q-PPhEK and A-PPhEK (colors range from light to dark representing 0.11 mol/L to 0.33 mol/L, 0.33 mol/L to 1 mol/L, 1 mol/L to 3 mol/L).

Q-PPhEK shows successional microstructure (Figs. 1e and g) while A-PPhEK exhibits a relatively discrete aggregating pattern (Figs. 1f and h) and there are some abrupt fluctuations on the surface morphology image as its longer side chain together with two oppositely charged functional groups. The ion cross-linking stem from the different aggregation microscopically between quaternary ammonium group and zwitterionic group thus resulting in more compact ion clusters.

To gain a deeper insight into the structure–activity relationship between ion exchange groups and membrane morphology, small-angle X-ray scattering (SAXS) was employed to estimate the ion cluster dimension (Fig. 2a). As shown in Fig. 2a, the scattering intensity of two membranes was located at 2.46 nm^{-1} and 1.67 nm^{-1}, and the corresponding d-spacing of ion cluster were calculated as 2.55 nm (A-PPhEK) and 3.76 nm (Q-PPhEK) respectively, which due to the distinguished aggregation caused by ionic cross-linked network. Despite featuring a high IEC, A-PPhEK does not have inter-connective ion channels. The cluster dimension of A-PPhEK is smaller than it of Q-PPhEK due to the ion cross-linking effect, which makes the ion clusters too compact to swell sufficiently in the solution thus leading an inefficient ion conduction. By contrast, the concentrated hydrophilic regions of Q-PPhEK can achieve an efficient ion conduction.

Based on the hydrophilic quaternary ammonium anchoring pendent alkyl side chains, proton could penetrate the Q-PPhEK membrane through aggregated ion channels. The proton transport rate is literally fast (3.62×10^{-3} cm^2 V^{-1} s^{-1}) and the ion channel dimension dominates ion transport especially at high concentration [44]. Notably, Donnan effect of Q-PPhEK membrane plays a critical part in vanadium ions inhibition comparing with Nafion. The vanadium resistance of all these membranes were verified by vanadium ion permeation test (Fig. 2b). Both VO^{2+} permeation rates of Q-PPhEK and A-PPhEK are lower than Nafion 115 implying that PPhEK membranes featuring better performance of vanadium resistance. From the perspective of continuous VO^{2+} concentration changes, the vanadium ions permeability of Q-PPhEK is the lightly higher than that of A-PPhEK, which is mainly guided by different ion cluster dimension.

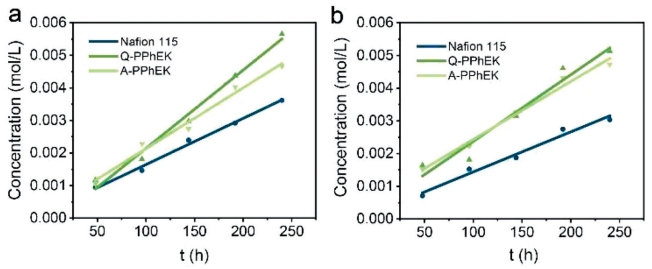

Fig. 3. Chemical stability of functionalized PPhEK membranes. (a) Oxidation test of Q-PPhEK, A-PPhEK and Nafion 115 in 0.15 mol/L VO_2^+. (b) Oxidation test of Q-PPhEK, A-PPhEK and Nafion 115 in 1.5 mol/L VO_2^+.

Ion-transport mechanism across PPhEK membranes was characterized by a four-electrode method and KCl was picked as a probe salt on account of the similar mobility of K^+ and Cl^- to figure out the different ion transport behavior of the PPhEK membranes [21]. As shown in Fig. 2c, the anionic Cl^- transport number (t_{Cl^-}) of Q-PPhEK is above 0.5, suggesting that the membranes are positively charged. With the KCl concentration gradually increasing from 0.11 mol/L to 3 mol/L, the anion/cation selectivity of the all PPhEK membranes decreases, t_{Cl^-} and t_{K^+} tend to equal, indicating that Donnan effect is weakened at high concentration. In virtue of above ion transport behavior, the conclusion has been drawn that, ion transport is no longer only controlled by Donnan effect but driven by the ion channel dimension and ion concentration of the solution. While the proton transport number was much higher than anion transport number in H_2SO_4 solution at all concentration, indicating that Q-PPhEK and A-PPhEK are prone to conduct protons in priority as protons' fast mobility (Fig. S10 in Supporting information) [12].

Oxidation stability of ICMs is a critical issue for VFBs practical application which highly determine the batteries lifetime. To verify the PPhEK stability, oxidation test of VO_2^+ was executed at the concentration of 0.15 mol/L and 1.5 mol/L, respectively (Figs. 3a and b). Q-PPhEK and A-PPhEK membranes withstood a long-term immersion in the highly acidic and oxidizing solution with no distinct changes in membrane morphology and chemical structures both in 0.15 mol/L and 1.5 mol/L VO_2^+ (Figs. S11 and S12 in Supporting information). The similar decomposition rate of PPhEK membranes comparing to the benchmark Nafion 115 have been validated, meaning that Q-PPhEK and A-PPhEK membranes are eligible for VFBs at both low and high oxidation concentrations (Figs. 3a and b). In a highly acidic environment, the oxygen atoms on polymer main chains could be protonated and served as strong electron-withdrawing groups (EWGs), together with strong EWGs (*e.g.*, sulfonic acid groups) directly anchored on the main chains, make the adjacent carbon atoms are easily attacked by vanadium(V) oxygen species thus leading a polymer degradation [20,45,46]. While the alkyl spacers effectively alleviated inductive withdrawing effect from ion exchange groups thus enabling the stable main chains.

VFB cells were assembled to estimate the battery performance of PPhEK membranes, as shown in Fig. 4. In terms of Q-PPhEK, the EEs at different current densities were over higher than A-PPhEK in which the EE of 90% and 82% was achieved at 80 and 160 mA/cm^2 respectively (Fig. 4a). The highest rate performance among PPhEK membranes should be attributed to the large ion channels. A-PPhEK shows a general R_A thus leading an EE of *ca.* 80% at 120 mA/cm^2. A lower EE at the same current density of A-PPhEK than Q-PPhEK should be attributed to the compact ion clusters (Fig. 4b). The smaller ion channels are not conducive to ion transport during charge and discharge process thus leading relatively lower VEs. Q-PPhEK and A-PPhEK are appointed for long-term cycling test at selected current density (160 and 120 mA/cm^2)

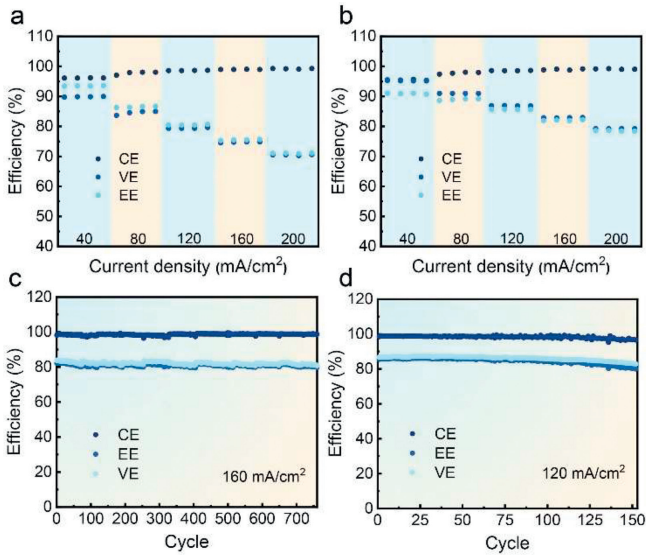

Fig. 4. Battery performance. (a) Rate performance of Q-PPhEK from 40 mA/cm^2 to 200 mA/cm^2. (b) Rate performance of A-PPhEK from 40 mA/cm^2 to 200 mA/cm^2. (c) Cycling performance of Q-PPhEK at 160 mA/cm^2. (d) Cycling performance of A-PPhEK at 120 mA/cm^2.

to maintain their EE above 80%. As shown in Figs. 4c and d, the cells with Q-PPhEK and A-PPhEK show EEs are above 80% while the corresponding CEs are nearly 100% over 750 and 150 cycles respectively. Apparently, a stable cell performance for a long period has been achieved especially by side-chain-type nonfluorinated Q-PPhEK membrane which is capable for VFBs as its improved ion selectivity, ion transport and stability.

In summary, two functionalized phenolphthalein-based cardo membranes bearing pendent alkyl chain terminated with ion exchange groups demonstrating elite stability under rigorous condition have been proved capable for VFBs. Alkyl spacers that effectively retarded electron withdrawing effect from EWGs, enable a stable backbone by the side chain strategy. The VFB cell assembled with Q-PPhEK membrane deliver an EE above 80% at 160 mA/cm^2 over 750 cycles. Different ion cluster dimension and membrane morphology are the pivotal factors leading to the different battery performance, hence more microstructures should be taken into consideration to adjust ion channels in membranes from the perspective of structure-activity relationship thus leading an improve battery performance. Based on this design, the aliphatic side chains act as buffer zone separating the ionic group from polymer backbone to keep the main chain inert that escape from severe decomposition and more kinds of backbone could be considered. More phenolphthalein-based membranes and other side-chain-types polymers with and remarkable stability, selectivity, conductivity, and cost-effectiveness are expected to be designed and applied to VFBs.

Declaration of competing interest

The authors declare that they have no known competing financial interests or personal relationships that could have appeared to influence the work reported in this paper.

Acknowledgments

The authors gratefully acknowledge the financial support of the National Natural Science Foundation of China (Nos. 22075276, U19A2016, U22B6012), CAS Strategic Leading Science & Technology Program (A) (No. XDA21070000), Dalian High Level Talent Innovation Support Program (No. 2020RD05), the Development of Scientic and Technological Project of the Jilin Province (No. 20210101126JC), International Partnership Program of Chinese Academy of Sciences (No. 121421KYSB20210028).

Supplementary materials

Supplementary material associated with this article can be found, in the online version, at doi:10.1016/j.cclet.2023.109231.

References

[1] Z. Yang, J. Zhang, M. Kintner-Meyer, et al., Chem. Rev. 111 (2011) 3577–3613.
[2] Y. Liu, Z. Yu, J. Chen, et al., Chin. Chem. Lett. 33 (2022) 1817–1830.
[3] S. Sabihuddin, A. Kiprakis, M. Mueller, Energies 8 (2015) 172–216.
[4] Z. Zhu, T. Jiang, M. Ali, et al., Chem. Rev. 122 (2022) 16610–16751.
[5] S. Guo, Y. Yu, Q. Zhang, Chin. Chem. Lett. 28 (2017) 2169–2170.
[6] M. Park, J. Ryu, W. Wang, J. Cho, Nat. Rev. Mater. 2 (2017) 16080.
[7] X. Li, H. Zhang, Z. Mai, H. Zhang, I. Vankelecom, Energy Environ. Sci. 4 (2011) 1147–1160.
[8] A. Weber, M. Mench, J. Meyers, et al., J. Appl. Electrochem. 41 (2011) 1137–1164.
[9] M. Skyllas-Kazacos, F. Grossmith, J. Electrochem. Soc. 134 (1987) 2950–2953.
[10] P. Xiong, L. Zhang, Y. Chen, S. Peng, G. Yu, Angew. Chem. Int. Ed. 60 (2021) 24770–24798.
[11] X. Ran, C. Yan, H. Zhang, et al., Chin. Chem. Lett. 18 (2007) 1269–1272.
[12] Q. Dai, Z. Zhao, M. Shi, et al., J. Membr. Sci. 632 (2021) 119335.
[13] S. Maurya, S. Shin, Y. Kim, S. Moon, RSC Adv. 5 (2015) 37206–37230.
[14] Z. Zhao, X. Liu, M. Zhang, et al., Chem. Soc. Rev. 52 (2023) 6031–6074.
[15] C. Ding, H. Zhang, X. Li, T. Liu, F. Xing, J. Phys. Chem. Lett. 4 (2013) 1281–1294.
[16] R. Potash, J. McKone, S. Conte, H. Abruna, J. Electrochem. Soc. 163 (2016) A338–A344.
[17] M. Skyllas-Kazacos, M. Chakrabarti, S. Hajimolana, F. Mjalli, M. Saleem, J. Electrochem. Soc. 158 (2011) R55–R79.
[18] B. Schwenzer, J. Zhang, S. Kim, et al., ChemSusChem 4 (2011) 1388–1406.
[19] Y. Xing, L. Liu, C. Wang, N. Li, J. Mater. Chem. A 6 (2018) 22778–22789.
[20] Z. Yuan, X. Li, J. Hu, et al., Phys. Chem. Chem. Phys. 16 (2014) 19841–19847.
[21] Z. Zhao, Q. Dai, X. Li, et al., J. Mater. Chem. A 10 (2022) 762–771.
[22] K. Mauritz, R. Moore, Chem. Rev. 104 (2004) 4535–4585.
[23] J. Kim, S. So, H. Kim, S. Choi, ACS Energy Lett. 6 (2021) 184–192.
[24] W. Hsu, T. Gierke, J. Membr. Sci. 13 (1983) 307–326.
[25] T. Gierke, G. Munn, F. Wilson, J. Polym. Sci. Polym. Phys. 19 (1981) 1687–1704.
[26] H. Mendil-Jakani, S. Pouget, G. Gebel, P. Pintauro, Polymer 63 (2015) 99–107.
[27] H. Yeager, A. Steck, J. Electrochem. Soc. 128 (1981) 1880–1884.
[28] M. Petersen, G. Voth, J. Phys. Chem. B 110 (2006) 18594–18600.
[29] R. Liu, J. Wang, X. Che, et al., J. Memb. Sci. 636 (2021) 119584.
[30] F. Bu, Y. Zhang, L. Hong, et al., J. Membr. Sci. 545 (2018) 167–175.
[31] N. Zhang, B. Wang, C. Zhao, et al., J. Mater. Chem. A 2 (2014) 13996–14003.
[32] J. Yang, Y. Wang, G. Yang, S. Zhan, Int. J. Hydrog. Energy 43 (2018) 8464–8473.
[33] Y. Sun, S. Zhou, G. Qin, et al., J. Membr. Sci. 620 (2021) 118899.
[34] K.J. Dahl, V. Jansons, Poly(arylene ether ketone) chemistry: Recent advances in synthesis and applications, in: P.N. Prasad, J.E. Mark, T.J. Fai (Eds.), Polymers and Other Advanced Materials: Emerging Technologies and Business Opportunities, Springer, Boston, 1995, pp. 69–81.
[35] G. Chen, X. Zhang, S. Zhang, T. Chen, Y. Wu, J. Appl. Polym. Sci. 106 (2007) 2808–2816.
[36] Q. Zhang, Q. Zhang, S. Zhang, S. Li, J. Membr. Sci. 354 (2010) 23–31.
[37] S. Nunez, C. Capparelli, M. Hickner, Chem. Mater. 28 (2016) 2589–2598.
[38] E. Park, Y. Kim, J. Mater. Chem. A 6 (2018) 15456–15477.
[39] L. Wu, T. Xu, D. Wu, X. Zheng, J. Membr. Sci. 310 (2008) 577–585.
[40] X. Yan, H. Zhang, Z. Hu, et al., ACS Appl. Mater. Interfaces 11 (2019) 44315–44324.
[41] H. Zhang, X. Yan, L. Gao, et al., ACS Appl. Mater. Interfaces 11 (2019) 5003–5014.
[42] L. Liu, C. Wang, Z. He, et al., J. Mater. Sci. Technol. 69 (2021) 212–227.
[43] T. Tran, C. Lin, S. Chaurasia, H. Lin, J. Membr. Sci. 574 (2019) 299–308.
[44] N. Agmon, H.J. Bakker, R.K. Campen, et al., Chem. Rev. 116 (2016) 7642–7672.
[45] Z. Yuan, X. Li, Y. Zhao, H. Zhang, ACS Appl. Mater. Interfaces 7 (2015) 19446–19454.
[46] D. Chen, M.A. Hickner, Phys. Chem. Chem. Phys. 15 (2013) 11299–11305.